Acta Crystallographica Section B
Structural Science
ISSN 0108-7681

Multipole refinement and electron density analysis in natural borosilicate datolite using X-ray diffraction data

Yu. V. Ivanov[a]* and E. L. Belokoneva[b]

[a]Russian State Library, 3/5 Vozdvizhenka Street, Moscow 119019, Russia, and [b]Department of Crystallography and Crystal Chemistry, Moscow State University, Leninskiye Gory, Moscow 119992 GSP-2, Russia

Correspondence e-mail: temples@yandex.ru

Received 17 July 2006
Accepted 9 October 2006

The electron density distribution in the layer silicate datolite, Ca[BOH(SiO_4)], was analyzed using high-precision single-crystal X-ray diffraction data (Mo $K\alpha$, T = 293 K). The Hansen–Coppens multipole model and Bader's topological analysis of the electron density provides a basis for the quantitative characterization of the bonded interaction of datolite. The results are presented both in the form of maps of the electron density distribution and its Laplacian, and in a compact way in terms of the critical points of the electron density. The relative electronegativities are also discussed. It was shown that closed-shell type interactions exist between Ca and O atoms, whereas Si—O and B—O bonds exhibit an intermediate nature with a strong covalent component. An analysis of the topology of the electrostatic potential demonstrates the relevance of considering this physical property to obtain a complete picture of structure-forming factors.

1. Introduction

Classical investigations of the structural chemistry of silicates were surveyed most completely in the monograph of Liebau (1985). The chemical bonding and its peculiarities in silicates were raised in that monograph. Several reviews of electron density (ED) investigations based on precise X-ray diffraction data (Tsirelson *et al.*, 1990; Gibbs *et al.*, 1994; Belokoneva, 1999) summarize the achievements in this field. Bonded radii, charges on atoms and bond ionicities in SiO_4, AlO_4, BO_4 and BeO_4 tetrahedra were estimated from the deformation electron density maps in relation to the electronic structure of the atoms and their electronegativities. New possibilities to solve the problems of isomorphism and to investigate hydrogen bonds were demonstrated. It was noted that the electron density distributions allow the fundamentals of the traditional structural chemistry of silicates to be studied at an electronic level. The list of compounds has been extended in recent years to include spodumene (Kuntzinger & Ghermani, 1999). Further, detailed topological analysis of the ED has been carried out for the zeolite minerals natrolite, mesolite, scolecite (Kirfel & Gibbs, 2000), stishovite (Kirfel *et al.*, 2001) and coesite (Gibbs *et al.*, 2003). A paper summarizing the experimental and theoretical bond critical point properties in a topological analysis of ED for the minerals has been published recently (Gibbs *et al.*, 2005). Among the compounds under investigation were orthosilicates (olivines, spinels, phenakite, euclase, eulitine, topaz, sphene), ring silicates ($KSiSi_3O_9$ wadeite-like, beryl, cordierite, dioptase, tourmaline), chain and band silicates (orthopyroxenes, clinopyroxenes, pectolite, andalusite), and framework silicates (quartz, coesite, danburite, natrolite, mesolite, scolecite). Layer silicates have

Table 1
Experimental details.

Crystal data	
Chemical formula	$BCaHO_5Si$
M_r	159.99
Cell setting, space group	Monoclinic, $P2_1/a$
Temperature (K)	293
a, b, c (Å)	9.646 (6), 7.620 (4), 4.839 (3)
β (°)	90.14 (5)
V (Å^3)	355.7 (4)
Z	4
D_x (Mg m^{-3})	2.988
Radiation type	Mo $K\alpha$
μ (mm^{-1})	1.99
Crystal form, colour	Sphere, pale green
Crystal size (mm)	0.25 × 0.25 × 0.25
Data collection	
Diffractometer	Syntax P-1
Monochromator	Graphite plate
Data collection method	Integrated intensities data from $\theta/2\theta$ scans
Absorption correction	For a sphere
T_{min}	0.608
T_{max}	0.614
No. of measured, independent and observed reflections	6018, 2584, 2584
Criterion for observed reflections	$I > 1.96\,\sigma(I)$
R_{int}	0.026
θ_{max} (°)	50.1
No. and frequency of standard reflections	1 every 100 reflections
Intensity decay (%)	No decay, variation 2
Refinement	
Refinement on	F
$R[F^2 > 2\sigma(F^2)]$, $wR(F^2)$, S	0.014, 0.019, 1.04
No. of reflections	2583
No. of parameters	267
Weighting scheme	$w = 1/[\sigma^2(F_{obs}) + (0.015F_{obs})^2]$
$(\Delta/\sigma)_{max}$	< 0.0001
$\Delta\rho_{max}$, $\Delta\rho_{min}$ (e Å^{-3})	0.63, −0.36
Extinction method	Becker–Coppens type 1 isotropic
Extinction coefficient	0.56 (2)

Computer programs used: *PROFIT* (Streltsov & Zavodnik, 1989), *MOLDOS*97 (Protas, 1997*a*), *SALDOS*97 (Protas, 1997*b*), *XPROP*98 (Ivanov *et al.*, 1997).

not yet been investigated. An explanation for this fact is the perfect cleavage typical of layered structures, which leads to diffuse effects in the diffraction which are not possible to avoid or correctly take into account; thus, accurate experimental data are not available. Borosilicates have not yet been studied, except tourmaline (Belokoneva & Tsirelson, 1993) and danburite (Downs & Swope, 1992). Interest in analyzing the ED in datolite $Ca[BOH(SiO_4)]$ stems from its structure in which the silicon–boron–oxygen $[BSiO_5]_{\infty\infty}$ layers consist of tetrahedra linked *via* shared vertices. BO_4 tetrahedra are oriented up and down the layer surface with one at their apices – the (OH) group – whereas the SiO_4 tetrahedra are oriented with two of its edges parallel to the layer surfaces. The anionic tetrahedral layer alternates along the z axis with the Ca-cationic layer, which is built from CaO_8 Thomson cube polyhedra. Datolite belongs to the mineralogical group of datolite–gadolinite–herderite minerals with the common formula $A_2BC_2D_2X_{10}$, for which mixed-valence isomorphic substitutions are typical. Apart from the Thomson cubes, the octahedral holes in the cationic layer are empty in datolite and are occupied by iron in gadolinite $Y_2FeBe_2Si_2O_{10}$. A previous study of the ED in datolite (Belokoneva & Goryunova, 1998) was performed using accurate X-ray diffraction data. A spherical-atom model was refined with high-angle data and dynamic Fourier-deformation ED maps were calculated. The present paper describes a multipole refinement of the ED using the same data set. Analysis of static multipole deformation ED maps, and topological analysis of the model ED and electrostatic potential (ESP) calculation have been carried out.

2. Experimental

A brief summary of the original experimental procedure is given below, so the experimental data set may be more easily understood. A specimen, prepared from a crystal of datolite from datolite–hedenbergite scarn deposit (Tetyche, Sikhote-Alin mountains), was used for the data collection. The crystal quality proved to be satisfactory as judged by the Laue X-ray diffraction patterns, which showed no diffuse scattering. The unit-cell parameters were refined from 15 high-angle reflections using monochromated Mo $K\alpha$ radiation on a four-circle Syntex $P\bar{1}$ diffractometer. The values obtained (Table 1[1]) agree with data reported previously for datolite (Foit *et al.*, 1973). The reflection profiles were step-scanned in the $2\theta/\theta$ mode; the scan speed varied from 2 to 12° min^{-1}. One standard reflection $(12\bar{1})$ was measured every 100 reflections; its intensity variation did not exceed 2%. The main data set was collected in the hemisphere h^0_+, k^-_+, l^-_+, where 4948 reflections were measured in the region 2θ = 5–100°. Then a further 1070 reflections were added in the region h^-_{-1}, k^-_+, l^-_+, 2θ = 5–50°. Thus, we obtained eight equivalents in the region 2θ = 5–50° and four in the region 2θ = 5–100°. The integrated intensities were determined by the Lehmann–Larsen procedure for peak profile analysis adopted in the program *PROFIT* (Streltsov & Zavodnik, 1989), which allows the intensity of weak reflections to be determined with greater accuracy. Two data sets were merged into one, which contained 6018 reflections including standards. The absorption correction for the sample under study was small (μr = 0.24) and did not affect the intensities, although this correction was still applied. Averaging the intensities of symmetry-equivalent reflections corrected for Lorenz and the polarization factor, $R_{int} = \sum_i(I_i - \langle I\rangle)/\sum_i\langle I\rangle_i$, showed that there are 51 weak reflections (less than 1% of the total number) with intensities which are out of this group. After the rejection of these reflections, averaging (R_{int} = 0.0259) led to a final data set of 2584 independent reflections. Systematic extinctions confirmed the space group of datolite to be $P12_1/a1$ ($P2_1/c$ in a standard setting). Microimpurities of sodium (0.21 at. %) and iron (0.42 at. %) were detected in our specimen and taken into account in the structural model

[1] Supplementary data for this paper are available from the IUCr electronic archives (Reference: AV5071). Services for accessing these data are described at the back of the journal.

Table 2
P_v, net charges and κ' parameters for datolite atoms obtained from κ refinement.

Atom	P_v	q	κ'
B	2.02 (9)	+0.98 (9)	1.20 (2)
Si	3.62 (16)	+0.38 (16)	1.025 (12)
O1	6.68 (4)	−0.68 (4)	0.955 (2)
O2	6.67 (4)	−0.67 (4)	
O3	6.84 (4)	−0.84 (4)	
O4	6.84 (4)	−0.84 (4)	
O5	6.68 (4)	−0.68 (4)	
Ca	0.09 (20)	+1.91 (20)	1.0 (fixed)
H	0.57 (6)	+0.43 (6)	1.45 (11)

earlier (Belokoneva & Goryunova, 1998). Therefore, the final structural formula of the mineral is $(Ca_{0.986}Na_{0.014})$-$Fe_{0.012}H_{0.988}[BSiO_5]$. A small amount of iron was found in an octahedral position, which is typically empty in datolite. The hydrogen bonds were examined on the basis of the ED maps and characterized as bifurcated bonds (Belokoneva & Goryunova, 1998). Crystallographic data and experimental information are summarized in Table 1.

3. Refinement

The static crystal ED was approximated by the multipole model of Hansen & Coppens (1978) as the sum of the pseudo-atomic electron densities, which are defined as

$$\rho_{\rm pseudoat}(\mathbf{r}) = \rho_{\rm core}(r) + P_v\kappa^3\rho_v(\kappa r) + \sum_{l=1}^{4}\kappa'^3 R_l(\kappa' r)\sum_{m=-l}^{l} P_{lm}y_{lm}(\mathbf{r}/r).$$

Refinements, based on $|F|$, were carried out using the program *MOLDOS*97 (Protas, 1997*a*; Hansen & Coppens, 1978). The neutral atom wavefunctions by Clementi & Roetti (1974) were used to calculate the core and valence form factors of all the atoms. The optimized parameters were the scale factor, the valence-shell populations P_v and the corresponding contraction–expansion parameters κ, the multipole populations P_{lm} (up to the hexadecapole level, $l_{\rm max} = 4$) and the corresponding contraction–expansion parameters κ'. The asymmetric unit was constrained to be neutral during the refinement of P_v. The multipole populations of the Ca ion were not refined because of the sharpness of their valence scattering factor, which would affect only very few low-order data. The presence of Fe^{2+} and Na^+ ions was neglected because of its low concentrations. The H-atom coordinates were fixed at values determined by nuclear magnetic resonance (Sugitani *et al.*, 1972). Isotropic secondary extinction according to Becker & Coppens (1974) was assumed to be mosaic-spread dominated (type I) with a Lorentzian distribution of the mosaic block orientation. The anomalous dispersion coefficients were taken from *International Tables for X-ray Crystallography* (1974). The exponential radial functions $R_l(\kappa' r) = r^{n_l}\exp(-\kappa'\xi r)$, with n_l = 1,2 for H, n_l = 2,2,3,4 for B and O, and n_l = 4,4,4,4 for Si, were used. Initial values for the orbital exponent coefficients $\xi_B = 2.5$, $\xi_{Si} = 3.5$, $\xi_O = 4.5$, $\xi_H = 2.2$ were selected according to Hehre *et al.* (1969). The same sets of κ and κ' parameters were used for all the O atoms. Starting atomic positional and displacement parameters were taken from Belokoneva & Goryunova (1998). The high-angle refinement of these parameters using free-atom scattering factors has been carried out using the *MOLDOS* program for comparison and demonstrated the agreement with the previous results obtained with the CSD program (Belokoneva & Goryunova, 1998). The final multipole refinement procedure was then applied using all reflections. First, the scale factor, extinction coefficient, and positional and anisotropic displacement parameters were fitted. Then ED parameters (P_v, κ, multipoles P_{lm} and κ') were obtained in several steps, to avoid correlations sets of κ and κ' which were refined separately. During this procedure one weak reflection was rejected. The correctness of the weighting scheme was checked by using the statistical test of Abrahams & Keve (1971). Figures of merit are given in Table 1. The positional and anisotropic displacement parameters are available in the supplementary material.

4. Results and discussion

Maps of the static deformation ED, $\delta\rho$, characterizing the redistribution of electrons during chemical bonding, were calculated using the *SALDOS*97 program (Protas, 1997*b*). The peak heights on the four Si—O bonds are in the range 0.32–0.54 e Å^{-3}, whereas the range of peak heights on B—O bonds is wider: 0.24–0.63 e Å^{-3} (Fig. 1). It is known that the atomic charges are relative values, which also depend on the method of determination. Nevertheless, this characteristic is of interest in solids. Experimental determinations of the effective atomic charges in ED investigations of compounds with the rock-forming elements such as Si, Al, Mg, Fe *etc.* have shown that the formal valence state is not realised. For example, the most typical charge for a Si atom lies in the range +1.1 to +1.8 e (Belokoneva, 1999). For comparison, the atomic net charges in datolite were determined using the special procedure of so-called 'kappa refinement' (Coppens *et al.*, 1979); the results are listed in Table 2. These charges are less than expected, especially for the Si atom (Table 2), which may be due to the layer character of the structure and the unusual bonding inside the SiO_4 tetrahedra with the absence of a shared interaction for every tetrahedral apex. In contrast to all known silicates (borosilicates), the SiO_4 tetrahedron possesses edges O2—O3 and O1—O4, which are parallel to the layer surfaces. Thus, strong interactions are only present inside the layer, which may lead to the accumulation of ED on the Si atom and a decrease in silicon-bonded charge.

The total ED may also be described in terms of the ED critical points (CPs), where the gradient of the ED, $\nabla\rho$, vanishes. The ED exhibits four kinds of nondegenerate CPs of rank 3: maxima (3,−3), two types of saddle points (3,−1) and (3,+1), and minima (3,+3). They correspond to nuclear positions, bonds, and rings and cages of atoms. The Laplacian of the ED, $\nabla^2\rho$, is also used to emphasize the fine details of the ED. If $\nabla^2\rho(\mathbf{r}) < 0$, then ED is locally concentrated in $\mathbf{r}$; if

Table 3
Parameters of the bond critical points in crystals of datolite and cation electronegativities for Si and B atoms.

Bond	x	y	z	R_{ij} (Å)	d_1 (Å)	d_2 (Å)	δ (Å)	ρ (e Å^{-3})	$\nabla^2\rho$ (e Å^{-5})	λ_1 (e Å^{-5})	λ_2 (e Å^{-5})	λ_3 (e Å^{-5})	$\lvert\lambda_1\rvert/\lambda_3$	h_e (a.u.)	χ_M
Si—O1	0.0668	0.3224	0.3689	1.575	0.668	0.909	0.028	1.313	15.6	−10.0	−8.95	34.52	0.290	−0.134	1.96
Si—O2	0.0305	0.2348	0.5501	1.649	0.695	0.956	0.029	0.949	14.3	−6.38	−5.75	26.46	0.241	−0.060	1.80
Si—O3	0.1337	0.3008	0.5561	1.656	0.688	0.972	0.056	1.114	11.2	−8.64	−6.98	26.77	0.323	−0.104	1.86
Si—O4	0.1122	0.1916	0.4109	1.660	0.688	0.974	0.036	1.088	11.8	−8.44	−6.66	26.93	0.313	−0.097	1.85
B—O2	0.3818	0.3760	0.5914	1.484	0.489	1.000	0.057	1.133	6.99	−8.64	−5.62	21.26	0.406	−0.122	1.74
B—O3	0.2986	0.3838	0.6025	1.479	0.485	0.994	0.016	0.942	12.4	−7.39	−5.47	25.24	0.293	−0.065	1.67
B—O4	0.3462	0.4677	0.6081	1.471	0.479	0.991	0.015	1.138	11.5	−8.22	−7.09	26.78	0.307	−0.108	1.74
B—O5	0.3409	0.4081	0.4678	1.498	0.484	1.014	0.029	1.024	12.6	−7.13	−5.35	25.07	0.284	−0.080	1.69
Ca—O1	0.4041	0.0107	0.8690	2.280	1.146	1.139	0.078	0.314	5.47	−1.51	−1.31	8.28	0.182	0.002	
Ca—O1′	0.4345	0.1009	1.1172	2.283	1.127	1.157	0.020	0.360	5.46	−1.89	−1.79	9.14	0.207	−0.003	
Ca—O2	0.3991	0.2046	0.8370	2.450	1.223	1.229	0.038	0.188	3.61	−0.87	−0.72	5.20	0.167	0.005	
Ca—O3′	0.3196	−0.0215	1.1681	2.661	1.304	1.364	0.097	0.135	2.04	−0.47	−0.41	2.91	0.162	0.003	
Ca—O3	0.2710	0.2170	0.8396	2.615	1.283	1.333	0.039	0.145	2.27	−0.62	−0.43	3.33	0.186	0.003	
Ca—O4	0.2385	0.0967	1.1455	2.418	1.203	1.216	0.044	0.222	3.78	−1.06	−0.84	5.68	0.187	0.003	
Ca—O5	0.2552	0.0041	0.8699	2.528	1.248	1.284	0.068	0.170	3.02	−0.73	−0.59	4.34	0.168	0.004	
Ca—O5′	0.3416	0.2594	1.1217	2.674	1.328	1.348	0.051	0.114	1.81	−0.39	−0.38	2.58	0.151	0.003	
O5—H	0.3953	0.4402	0.2007	0.913	0.662	0.252	0.032	2.944	−32.2	−47.8	−45.2	60.9	0.786	−0.832	

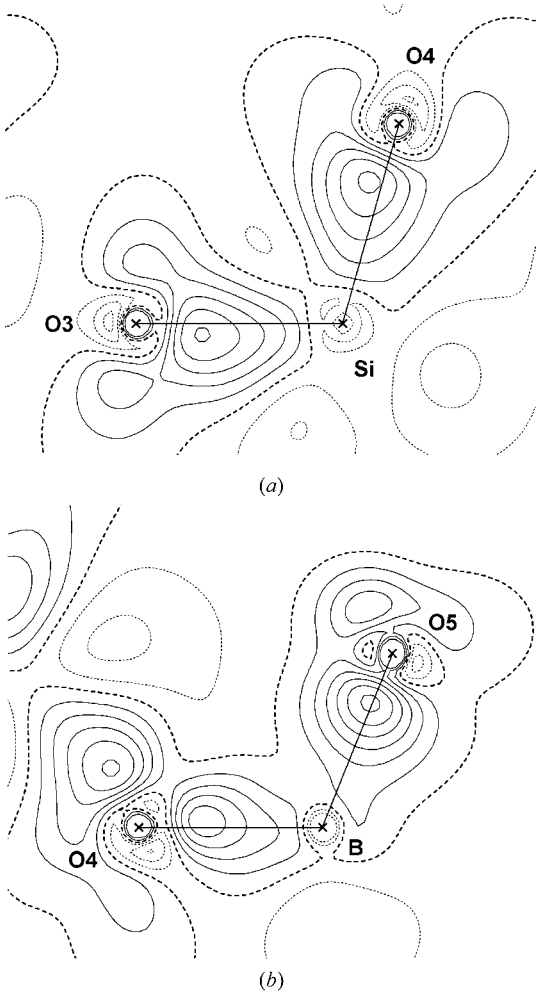

Figure 1
The static model-deformation ED in the structural polyhedra of datolite. The contour interval is 0.1 e Å^{-3}. The positive contours are solid, the negative contours are dashed and the zero level is bold-dashed. Contours in the vicinity of the atomic positions are omitted. (*a*) Section O3—Si—O4. (*b*) Section O4—B—O5.

$\nabla^2\rho(\mathbf{r}) > 0$, then $\rho(\mathbf{r})$ is locally depleted (Bader, 1990; Tsirelson & Ozerov, 1996). A topological analysis of the ED of datolite was performed using the *XPRO*98 program (Ivanov *et al.*, 1997). According to Bader (1990), the low value of the ED and the positive Laplacian value of the ED at the bond CP correspond to a predominantly closed-shell interaction between bonded atoms. Moreover, the recent analysis of the literature data has shown that the (3,−1) CPs of the bonds, usually described as ionic, are characterized by $0.07 < \rho(\mathbf{r}_{cp}) < 0.25$ e Å^{-3} and $0.12 < |\lambda_1|/\lambda_3 < 0.17$, where λ_1 and λ_3 are the first and third curvatures of the ED at the CP (Tsirelson, 1999). Analysis of the values of the kinetic electronic energy density, $g(\mathbf{r})$, the potential electronic energy density, $v(\mathbf{r})$, and the density of the total electronic energy, $h_e(\mathbf{r}) = g(\mathbf{r}) + v(\mathbf{r})$ (Bader & Beddall, 1972), gives us an additional method of attributing the atomic interactions. According to Cremer & Kraka (1984), at the bond CP $h_e(\mathbf{r}_{cp}) < 0$ for shared interactions and $h_e(\mathbf{r}_{cp}) > 0$ for closed-shell interactions. A gradient expansion (Kirzhnits, 1957) that is more adequate than the Yang (1986) mean-path approximation (Abramov, 1997; Tsirelson, 2002) was used to calculate $g(\mathbf{r})$. The potential electronic energy density was obtained *via* the local form of the virial theorem $2g(\mathbf{r}) + v(\mathbf{r}) = \frac{1}{4}\nabla^2\rho(\mathbf{r})$ (Bader & Beddall, 1972; Bader, 1990). This method was discussed in detail by Tsirelson (2002). The above-mentioned characteristics of bond CPs are presented in Table 3; they lead to the conclusion that datolite possesses the closed-shell type interactions between Ca and O atoms, whereas Si—O and B—O bonds exhibit an intermediate nature with a strong covalent component. This difference in bond types clearly shows itself in $\nabla^2\rho$ maps (Fig. 2). As was noted by Popelier (2000) using a water molecule as an example, H and O atoms form a joint valence-shell charge concentration (VSCC) and a joint valence-shell charge depletion (VSCD). In the case of datolite this effect manifests itself on $\nabla^2\rho$ maps as a bridge of electron concentration between O5 and H (Fig. 2*a*). The shifts of the

CPs from the internuclear lines, δ, reflect the strain in the structure (Table 3).

As the Ca—O bonds in the Thomson cube have a significant range of bond lengths (2.280–2.674 Å), it was interesting to investigate their correlation with the bonded radii of O atoms, R_b(O). It was found that this dependence is practically linear, moreover, these R_b(O) values and other bonded radii of oxygen for B—O and Si—O bonds correspond well with the *ab initio* results of Gibbs *et al.* (2001) and Downs *et al.* (2002) (Fig. 3*a*). The same trend is also observed for the silicates danburite (Downs & Swope, 1992), coesite (Downs, 1995), topaz (Ivanov *et al.*, 1998), scolecite (Kuntzinger *et al.*, 1998), natrolite, mesolite and scolecite (Kirfel & Gibbs, 2000), stishovite (Kirfel *et al.*, 2001) and coesite (Gibbs *et al.*, 2003). The detailed description of this correlation was carried out recently (Gibbs *et al.*, 2005). The dependences of both theoretical and experimental $\rho(\mathbf{r}_{cp})$ and $\nabla^2\rho(\mathbf{r}_{cp})$ values *versus* bond length were also plotted (Figs. 3*b* and *c*). It was found that Ca—O bond lengths in datolite correlate with the theoretical trends with the Ca—O bond length decreasing as ED at CPs and Laplacian both increase in value. At the same time the parameters of CPs at B—O bonds do not demonstrate correlation between bond lengths and $\rho(\mathbf{r}_{cp})$ and $\nabla^2\rho(\mathbf{r}_{cp})$, as was found for framework borosilicate danburite (Downs & Swope, 1992). No correlation between R(Si—O) and CP

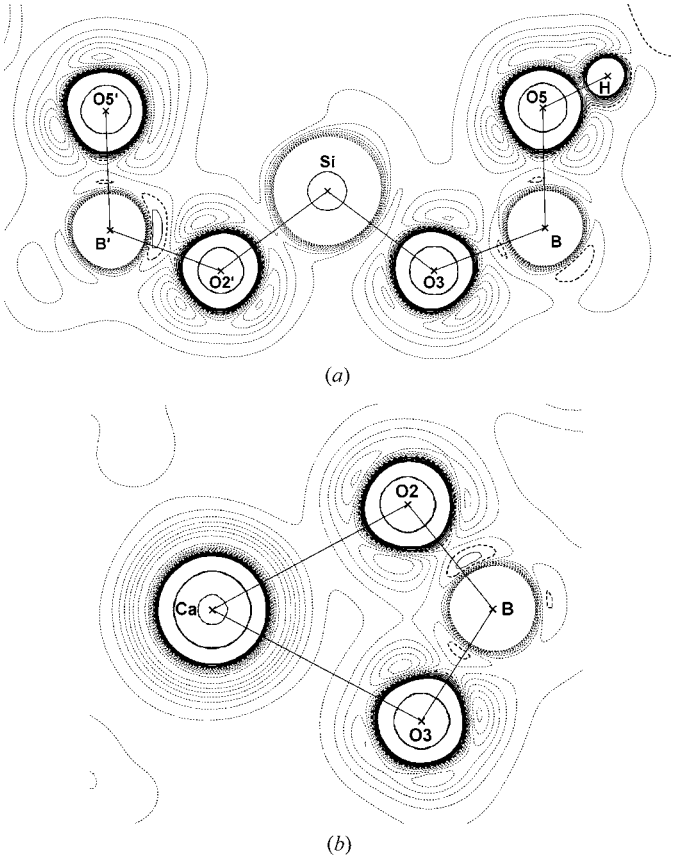

Figure 2
The Laplacian of the static model ED in datolite. Solid contours correspond to regions where the ED is locally concentrated, dashed lines are where the ED is locally depleted (2.5 e Å^{-5} interval). Contours from the innermost nodal surfaces are omitted. (*a*) Section O5′—B′—O2′—Si—O3—B—O5—H, averaged plane. (*b*) Section Ca—O2—B—O3, averaged plane.

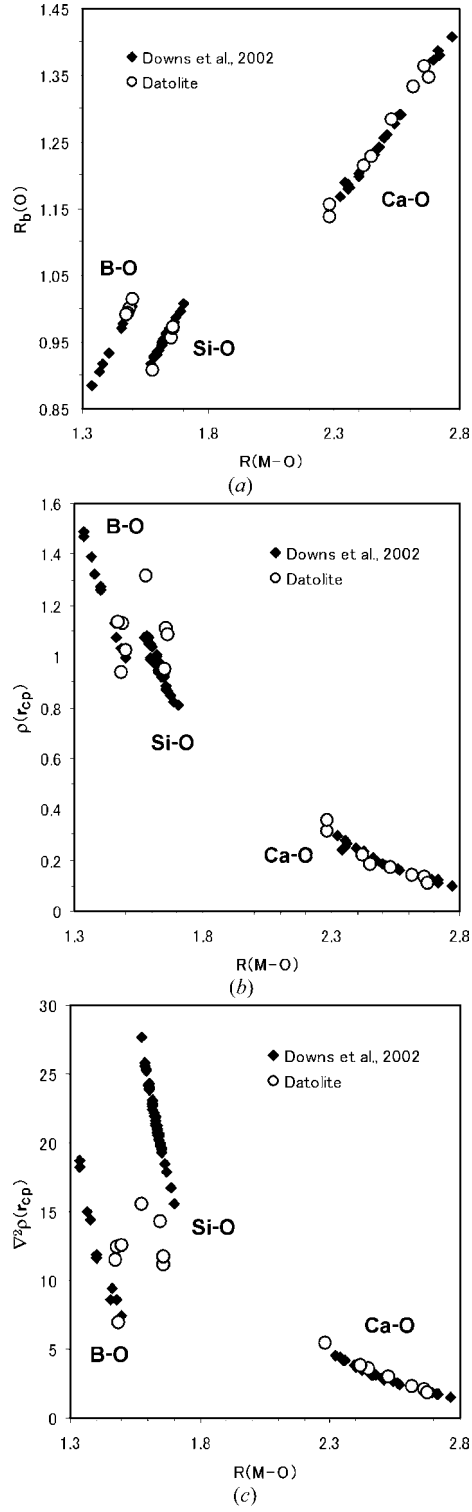

Figure 3
Bond CP properties *versus* the B—O, Si—O and Ca—O bond lengths (expressed in Å). Rhombi mark the *ab initio* points (Downs *et al.*, 2002). Circles mark datolite points. (*a*) Plot of R_b(O) (bonded radii) *versus* bond lengths. (*b*) Plot of $\rho(r_{cp})$, expressed in e Å^{-3}, *versus* bond lengths. (*c*) Plot of $\nabla^2\rho(r_{cp})$, expressed in e Å^{-5}, *versus* bond length.

Table 4
Topological atomic radii derived from the total ED (Bader's radii) and derived from the ESP.

Bond	Radius (Å)	Bond	Radius (Å)	Bond length (Å)		
Cation→anion	Bader's	ESP	Anion→cation	Bader's	ESP	
Si→O1	0.668	0.866	O1→Si	0.909	0.709	1.575
Si→O2	0.695	0.923	O2→Si	0.956	0.727	1.649
Si→O3	0.688	0.930	O3→Si	0.972	0.727	1.656
Si→O4	0.688	0.917	O4→Si	0.974	0.744	1.660
Mean for Si	0.685	0.909	Mean for O→Si	0.953	0.727	1.635
B→O2	0.489	0.761	O2→B	1.000	0.723	1.484
B→O3	0.485	0.764	O3→B	0.994	0.715	1.479
B→O4	0.479	0.752	O4→B	0.991	0.719	1.471
B→O5	0.484	0.772	O5→B	1.014	0.726	1.498
Mean for B	0.484	0.762	Mean for O→B	1.000	0.721	1.483
Ca→O1	1.146	1.328	O1→Ca	1.139	0.952	2.280
Ca→O1′	1.127	1.345	O1′→Ca	1.157	0.938	2.283
Ca→O2	1.223	1.448	O2→Ca	1.229	1.002	2.450
Ca→O3′	1.304	1.574	O3′→Ca	1.364	1.087	2.661
Ca→O3	1.283	1.587	O3→Ca	1.333	1.028	2.615
Ca→O4	1.203	1.403	O4→Ca	1.216	1.015	2.418
Ca→O5	1.248	1.541	O5→Ca	1.284	0.987	2.528
Ca→O5′	1.328	1.569	O5′→Ca	1.348	1.105	2.674
Mean for Ca	1.233	1.474	Mean for O→Ca	1.259	1.014	2.489
H→O5	0.253	0.319	O5→H	0.663	0.594	0.913
			Mean for O	1.091	0.853	

parameters was detected for datolite. It should be noted that for the Si—O bonded interactions the experimental values of $\nabla^2\rho(\mathbf{r}_{cp})$ are significantly smaller than the calculated values. All these unusual properties may also be connected with the unusual bonding inside the layered anionic unit, as was mentioned above. From the properties discussed R_b(O) is the most reproducible. Taking into account that the correlation between R_b(O) and $R(M—O)$ does not depend on the type of silicate, we suspect that similar averaged theoretical curves can be useful at least for the detection of random refinement blunders.

The electronegativity is regarded conventionally as a property which is independent of an atom's environment (Pauling, 1960). Nevertheless, it is possible to determine this atomic property *in situ*, depending on the valence state and the bonding of an atom. Relative electronegativities have been derived from the electron density topology analysis for silicates (Kirfel & Gibbs, 2000) and nitrides (Feth *et al.*, 1998). We developed the same approach for datolite. In the case of *M*—O bonds, electronegativity can be calculated from the parameters of CP by $\chi_M = 1.31[N_M\rho(\mathbf{r}_{cp})/R_b(O)]^{0.23}$ (Hill *et al.*, 1997), where N_M is the number of valence electrons on the first- or second-row *M* cations (Kirfel & Gibbs, 2000). The values of χ_{Si} obtained (Table 3) are in the range 1.80–1.96 (mean 1.87), which is in good agreement with experimental values: 1.72–1.96 (mean 1.85) by Kirfel & Gibbs (2000) for three zeolites (natrolite, mesolite and scolecite); with *ab initio* results: 1.72–2.00 (mean 1.82) by Hill *et al.* (1997); and with Pauling's value of 1.8 (Pauling, 1960). The electronegativity of the B atom (Table 3), 1.67–1.74, mean 1.71, is notably lower than the value of 2.0 proposed by Pauling (1960). At the same time it agrees with values calculated by Hill *et al.* (1997), 1.57–1.86 (mean 1.78), and with 1.66–1.75 (mean 1.71) obtained from danburite's data by Downs & Swope (1992).

The electrostatic potential (ESP) is also a very important inner-crystal scalar field, which has attracted more and more attention in recent years. The ESP is defined to within a constant. In practice, the evaluation of this constant presents some difficulties (Sommer-Larsen *et al.*, 1990; Becker & Coppens, 1990; O'Keeffe & Spence, 1994). Here, the optimal approach is the analysis of the topology of an ESP, which is similar to the topological analysis of ED. As well as in ED, there are four types of nondegenerate CPs in ESP: (3,−3), (3,−1), (3,+1) and (3,+3). In fact, the nuclei are not real (3,−3) CPs. However, the behavior of the ESP field close to the nuclear positions is indistinguishable from that for true maxima (Tal *et al.*, 1980) and they can be considered as the maxima in the ESP, with no other strict local maxima (Pathak & Gadre, 1990). It should be mentioned that the direct usage of the nomenclature of CP in ED for CP in ESP, namely 'ring CP' and 'cage CP', which can be found in the literature, is incorrect. The existence of 'ring' (3,+1) CP inside a ring of atoms and 'cage' (3,+3) CP in an interatomic hole is the result of monotonically decreasing the ED of atoms. A similar picture is expected for the topology of a nuclear potential. Really, the ESP of a cation

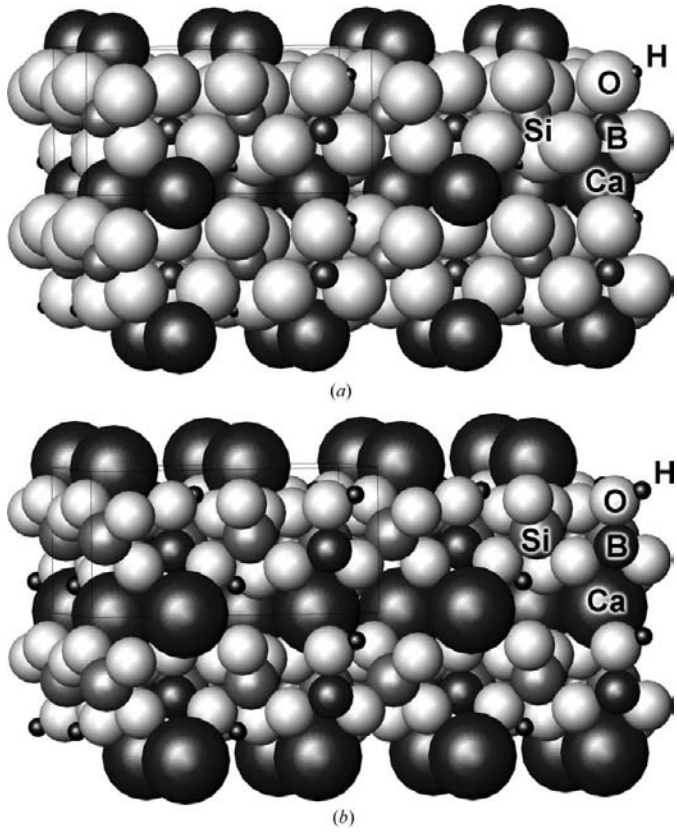

Figure 4
The ball model of the datolite structure. (*a*) Averaged Bader's topological radii are used. (*b*) Averaged ESP's radii are used.

is a monotonically decreasing function, whereas the ESP of an anion has a minimum at some distance from the nucleus (Sen & Politzer, 1989). It results in the formation of a complicated pattern of CPs; moreover, minima (3,+3) and saddles (3,+1) can appear not only in internuclear space. A good example is the water molecule, where two minima (3,+3) from lone electron pairs, and saddle (3,+1), connecting them, lie outside of the H—O—H triangle area (Gadre *et al.*, 1992; Leboeuf *et al.*, 1999). In connection with the complexity of the interpretation of ESP topology in a low-symmetry crystal like datolite, we confined ourselves to evident values, namely ESP bonded radii, which are defined as the distances between the bond CP and the nuclei of the bonded atoms. In all cases the bonded radii of the cations derived from the ESP are much larger than the bonded radii derived from the ED. The oxygen anions show the reverse picture (Table 4). Thus, in terms of ESP the customary concept of the crystal structure depicting the arrangement of small cations in holes between large adjoining anions is not justified (Spackman *et al.*, 1987). The notion of a cationic grid as a basis for the structure (Fig. 4) is more accurate here (Ivanov, 1998). The distortions of the anion layers are determined by both sizes (charges) of cations, and the spatial topology of the cationic grid. The role of the cationic grid (matrix) as a structure-forming factor was emphasized by Borisov & Podberezskaya (1984), Borisov (1996) and Vegas & Jansen (2002) for many classes of compounds.

The authors are grateful to Professor J. Protas and Professor N. K. Hansen for permission to use the *MOLDOS* program. Professor J. Protas is also thanked for helpful discussions.

References

Abrahams, S. C. & Keve, E. T. (1971). *Acta Cryst.* A**27**, 157–165.
Abramov, Yu. A. (1997). *Acta Cryst.* A**53**, 264–272.
Bader, R. F. W. (1990). *Atoms in Molecules: a Quantum Theory*. Oxford University Press.
Bader, R. F. W. & Beddall, P. M. (1972). *J. Chem. Phys.* **56**, 3320–3329.
Becker, P. & Coppens, P. (1974). *Acta Cryst.* A**30**, 129–147.
Becker, P. & Coppens, P. (1990). *Acta Cryst.* A**46**, 254–258.
Belokoneva, E. L. (1999). *Russ. Chem. Rev.* **68**, 299–316.
Belokoneva, E. L. & Goryunova, A. N. (1998). *Russ. J. Inorg. Chem.* **43**, 1915–1927.
Belokoneva, E. L. & Tsirelson, V. G. (1993). *Russ. J. Inorg. Chem.* **38**, 1351–1356.
Borisov, S. V. (1996). *J. Struct. Chem.* **37**, 773–779.
Borisov, S. V. & Podberezskaya, N. V. (1984). *The Stable Cationic Frames in Fluorides and Oxides*. Novosibirsk: Nauka.
Clementi, E. & Roetti, C. (1974). *At. Data Nucl. Data Tables*, **14**, 177–478.
Coppens, P., Guru Row, T. N., Leung, P., Stevens, E. D., Becker, P. J. & Yang, Y. W. (1979). *Acta Cryst.* A**35**, 63–72.
Cremer, D. & Kraka, E. (1984). *Croat. Chem. Acta*, **57**, 1259–1281.
Downs, J. W. (1995). *J. Phys. Chem.* **99**, 6849–6856.
Downs, R. T., Gibbs, G. V., Boisen, M. B. Jr & Rosso, K. M. (2002). *Phys. Chem. Miner.* **29**, 369–385.
Downs, J. W. & Swope, R. J. (1992). *J. Phys. Chem.* **96**, 4834–4840.
Feth, S., Gibbs, G. V., Boisen, M. B. Jr & Hill, F. C. (1998). *Phys. Chem. Miner.* **25**, 234–241.
Foit, F. F. Jr, Phillips, M. W. & Gibbs, G. V. (1973). *Am. Mineral.* **58**, 909–914.
Gadre, S. R., Kulkarni, S. A. & Shrivastava, I. H. (1992). *J. Chem. Phys.* **96**, 5253–5260.
Gibbs, G. V., Boisen, M. B. Jr, Beverly, L. L. & Rosso, K. M. (2001). *Rev. Mineral. Geochem.* **42**, 345–381.
Gibbs, G. V., Cox, D. F., Rosso, K. M., Kirfel, A., Lippmann, T., Blaha, P. & Schwarz, K. (2005). *Phys. Chem. Miner.* **32**, 114–125.
Gibbs, G. V., Downs, J. W. & Boisen, M. B. (1994). *Rev. Mineral.* **29**, 331–368.
Gibbs, G. V., Whitten, A. E., Spackman, M. A., Stimpfl, M., Downs, R. T. & Carducci, M. D. (2003). *J. Phys. Chem. B*, **107**, 12996–13006.
Hansen, N. K. & Coppens, P. (1978). *Acta Cryst.* A**34**, 909–921.
Hehre, W. J., Stewart, R. F. & Pople, J. A. (1969). *J. Chem. Phys.* **51**, 2657–2664.
Hill, F. C., Gibbs, G. V. & Boisen, M. B. Jr (1997). *Phys. Chem. Miner.* **24**, 582–596.
Ivanov, Yu. V. (1998). PhD Thesis. Mendeleev University of Chemical Technology of Russia. (Abstract is available online at: http://orel.rsl.ru/dissert/ivanov_y_v/content.htm.)
Ivanov, Yu., Abramov, Yu. & Tsirelson, V. (1997). *National Conference on Application of the X-ray, Neutrons and Electrons for Study of Materials. Abstracts*, p. 599. Dubna: JINR.
Ivanov, Yu. V., Belokoneva, E. L., Protas, J., Hansen, N. K & Tsirelson, V. G. (1998). *Acta Cryst.* B**54**, 774–781.
Kirfel, A. & Gibbs, G. V. (2000). *Phys. Chem. Miner.* **27**, 270–284.
Kirfel, A., Krane, H.-G., Blaha, P., Schwarz, K. & Lippmann, T. (2001). *Acta Cryst.* A**57**, 663–677.
Kirzhnits, D. A. (1957). *Sov. Phys. JETP*, **5**, 64–71.
Kuntzinger, S. & Ghermani, N. E. (1999). *Acta Cryst.* B**55**, 273–284.
Kuntzinger, S., Ghermani, N. E., Dusausoy, Y. & Lecomte, C. (1998). *Acta Cryst.* B**54**, 819–833.
Leboeuf, M., Köster, A. M., Jug, K. & Salahub, D. R. (1999). *J. Chem. Phys.* **111**, 4893–4905.
Liebau, F. (1985). *Structural Chemistry of Silicates.* Berlin, Heidelberg, New York: Springer-Verlag.
O'Keeffe, M. & Spence, J. C. H. (1994). *Acta Cryst.* A**50**, 33–45.
Pathak, R. K. & Gadre, S. R. (1990). *J. Chem. Phys.* **93**, 1770–1773.
Pauling, L. (1960). *The Nature of the Chemical Bond*, 3th Ed. Ithaca, New York: Cornell University Press.
Popelier, P. L. A. (2000). *Coord. Chem. Rev.* **197**, 169–189.
Protas, J. (1997*a*). *MOLDOS*97/*MOLLY* MS DOS Updated Version. Private communication.
Protas, J. (1997*b*). *SALDOS*97/*SALLY* MS DOS Updated Version. Private communication.
Sen, K. D. & Politzer, P. (1989). *J. Chem. Phys.* **90**, 4370–4372.
Sommer-Larsen, P., Kadziola, A. & Gajhede, M. (1990). *Acta Cryst.* A**46**, 343–351.
Spackman, M. A., Hill, R. J. & Gibbs, G. V. (1987). *Phys. Chem. Miner.* **14**, 139–150.
Streltsov, V. A. & Zavodnik, V. E. (1989). *Sov. Phys. Cryst.* **34**, 1369–1371.
Sugitani, Y., Watanabe, M. & Nagashima, K. (1972). *Acta Cryst.* B**28**, 326–327.
Tal, Y., Bader, R. F. W. & Erkku, R. (1980). *Phys. Rev. A*, **21**, 1–11.
Tsirelson, V. G. (1999). *Acta Cryst.* A**55**, Suppl., Abstr. M13.OF.003.
Tsirelson, V. G. (2002). *Acta Cryst.* B**58**, 632–639.
Tsirelson, V. G., Evdokimova, O. A., Belokoneva, E. L. & Urusov, V. S. (1990). *Phys. Chem. Miner.* **17**, 275–292.
Tsirelson, V. G. & Ozerov, R. P. (1996). *Electron Density and Bonding in Crystals.* Bristol, Philadelphia: IOP.
Vegas, A. & Jansen, M. (2002). *Acta Cryst.* B**58**, 38–51.
Yang, W. (1986). *Phys. Rev. A*, **34**, 4575–4585.